Free Radical Production by Sonolysis of Aqueous Mixtures of N,N-Dimethylformamide: An EPR Spin Trapping Study

ARTICLE *in* THE JOURNAL OF PHYSICAL CHEMISTRY · APRIL 1995

Impact Factor: 2.78 · DOI: 10.1021/j100016a037

3 AUTHORS, INCLUDING:

Louis Kirschenbaum
University of Rhode Island
62 PUBLICATIONS **989** CITATIONS
SEE PROFILE

Peter Riesz
U.S. Department of Health and Human Services
200 PUBLICATIONS **5,289** CITATIONS
SEE PROFILE

Reprinted from The Journal of Physical Chemistry, 1995, 99.

Free Radical Production by Sonolysis of Aqueous Mixtures of *N,N*-Dimethylformamide: An EPR Spin Trapping Study

Vladimír Mišík,[†,§] Louis J. Kirschenbaum,[‡] and Peter Riesz*[,†]

Radiation Biology Branch, National Cancer Institute, National Institutes of Health, Bethesda, Maryland 20892, and Department of Chemistry, University of Rhode Island, Kingston, Rhode Island 02881

Received: September 12, 1994; In Final Form: February 14, 1995[⊗]

The 50-kHz sonochemistry of argon-saturated aqueous mixtures of *N,N*-dimethylformamide (DMF) was investigated by spin trapping with EPR detection, using 3,5-dibromo-4-nitrosobenzene sulfonate (DBNBS) as the spin trap. Methyl radicals, produced by pyrolysis in the hot cavitation regions and $^{\bullet}CH_2N(CH_3)CHO$ radicals, formed by hydrogen abstraction from DMF, were spin trapped over a wide range of DMF concentrations (0.004−12.9 mol/L (100% DMF)). The thermal decomposition of the spin trap did not contribute to the observed radical yield. Sonochemical yields of both types of radical adducts increased with increasing DMF concentration in spite of the decreased production of $^{\bullet}H$ and $^{\bullet}OH$ radicals from the thermolysis of water. The increase of the radical yield is not due to the increased availability of the monomeric form of the spin trap at higher DMF concentrations but can be explained by an increased amount of DMF thermolysis in the hot cavitation region. This behavior is in contrast to that of aqueous mixtures of volatile solvents (solvents with vapor pressures higher than water), which show a maximum followed by a decrease of radical yields at higher mole fractions of the volatile component, due to the decrease of the effective $\gamma = C_p/C_v$ in the imploding cavitation bubbles.

Introduction

Ultrasound has been used extensively in organic synthesis to increase the yields and rates of both homogeneous and heterogeneous processes.[1−4] With the widespread use of *N,N*-dimethylformamide (DMF) as a solvent and catalyst in organic synthesis[5] the understanding of the radical processes triggered by ultrasound is of general interest because of potential side reactions initiated by radicals sonolytically produced from DMF. Sonolysis of aqueous DMF mixtures was shown to increase cell killing in a synergistic fashion.[6,7] This observation suggests a role for organic radicals derived from DMF in cell killing with possible implications for cancer treatment.

The chemical effects of ultrasound are due to the high temperatures (thousands of Kelvin)[8,9] and pressures (hundreds of atmospheres)[10] produced during violent collapse of acoustic cavitation bubbles. These collapsing microbubbles, filled with dissolved gas (i.e. argon) and solvent vapors, are the reaction microchambers in which solvent vapor can undergo pyrolysis, thus producing radicals that undergo further reactions. A thin shell of liquid surrounding the collapsing microbubbles experiences temperatures and pressures exceeding the critical temperatures and pressures of the liquid (these critical values are 374 °C and 221 atm for water); thus, a supercritical fluid is formed in this region.[11] The physical properties of the supercritical fluid differ from those of the bulk liquid. One of the most notable changes is the lowering of the dielectric constant of polar solvents such as water, which may enable accumulation of low-polarity solutes at this interface (the dielectric constant of water at 1000 °C and at density 1 g/cm^3 is 12 compared to a value of 90 at 0 °C; at the critical point, the dielectric constant is only 6).[12] Definitive evidence on the feasibility of diffusion to this region on the short time scale in which the supercritical fluid is formed during the final stages of bubble growth under the influence of the sound field (rectified diffusion) and during the collapse of the bubble is not available. An alternative mechanism to explain the well-established crucial role of the hydrophobicity of solutes for the susceptibility for sonochemical reactions is the favorable partitioning of the low-polarity substances at the bubble−water interface due to the hydrophobic interactions.[13,14] Thermolysis as well as radical abstraction reactions occur in this region. In the third region, which is the bulk liquid at ambient temperature, the free radicals formed in the hot cavitation regions which have not recombined or disproportionated and have not been scavenged react with the solutes to produce radicals by hydrogen abstraction and undergo reactions similar to those found in the radiation chemistry of liquids.[15−17]

The physicochemical properties of the liquids, such as viscosity, surface tension, sound velocity, ratio of the specific heats γ (C_p/C_v), thermal conductivity, hydrophobicity, and vapor pressure, are important parameters that determine the extent of acoustic cavitation and sonochemical yields. It was demonstrated experimentally by Suslick et al.[18] that an inverse relationship exists between the logarithm of the rates of sonochemical decomposition of alkanes and their vapor pressure. The sonolytic production of free radicals in aqueous mixtures of solutes of vapor pressure higher than water (e.g. acetone, acetonitrile, methanol, ethanol) has been studied previously using the EPR spin trapping technique.[19,20] It was observed that the pyrolysis radical yields (typically methyl) first incease with increasing concentrations of the solute available for pyrolysis in the gas bubbles and starts decreasing at higher mole fraction of the volatile component in the water, due to the lowering of the effective γ of the cavitation bubble. Contrary to these results, studies with nonvolatile solutes of low hydrophobicity, such as sodium acetate, sodium propionate, amino acids, and sugars, show formation of pyrolysis radicals

* Correspondence: Dr. Peter Riesz, NCI, NIH, Bldg. 10, Rm. B1B50, Bethesda, MD 20892. Fax: (301)480-2238. Phone: (301)496-4036. E-mail: sono@helix.nih.gov.
† National Institutes of Health.
‡ University of Rhode Island.
§ A Fogarty Visiting Fellow on leave from the Institute of Experimental Pharmacology, Slovak Academy of Sciences, Bratislava, Slovak Republic.
⊗ Abstract published in *Advance ACS Abstracts,* April 1, 1995.

0022-3654/95/2099-5970$09.00/0

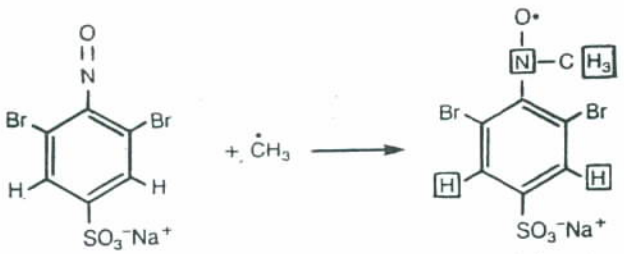

Figure 1. Example of spin trapping with 3,5-dibromo-4-nitrosobenzenesulfonic acid, sodium salt (DBNBS). The formation of a spin adduct with methyl radicals is shown. Shown in squares are the atoms that contribute to the hyperfine splittings.

only at high solute concentrations (typically >0.5 mol/L). Sonolysis of aqueous mixtures of dimethyl sulfoxide (DMSO), as an example of a solvent freely miscible with water, with vapor pressure lower than water but also sufficiently hydrophobic to allow partitioning in the region of low polarity at the bubble interface, was studied.[21] High yields of $^{\bullet}CH_3$ radicals were produced at low mole fraction of DMSO in water, not as a result of pyrolysis but due to the reaction with $^{\bullet}OH$ radicals. Their yields eventually decreased to zero at higher DMSO concentration with a concomitant appearance of $SO_3^{\bullet-}$ radicals, which were produced by oxidation of SO_2, a nonradical product of DMSO pyrolysis, by the spin trap DBNBS in the presence of water. Because of this complex chemistry, dependent on the reactions with the detector molecule and on the presence of water, it was desirable to study aqueous mixtures of another solvent with similar properties (freely miscible with water, vapor pressure lower than water, and higher hydrophobicity) but with simpler sonochemistry. Dimethylformamide fulfills these criteria and was therefore selected for this study.

Materials and Methods

Chemicals. *N,N*-Dimethylformamide (DMF, HPLC grade) was obtained from Aldrich Chemical Co. (Milwaukee, WI) and was dried over a molecular sieve, 3 Å (Aldrich). The deuterated *N,N*-dimethylformamide-d_7 (DMF-d_7; 99.5 atom % D) was from MSD Isotopes (St. Louis, MO). Milli-Q water was used in all experiments.

Spin Traps. The nitroso spin trap 3,5-dibromo-4-nitrosobenzene sulfonic acid, sodium salt (DBNBS; from OMRF Spin Trap Source, Oklahoma), was used to measure the radicals produced by sonolysis of aqueous solutions of DMF (Figure 1). The 2,6-deuterated analogue, DBNBS-d_2, obtained from Dr. M. R. Chedekel (Melanin Laboratories, The Johns Hopkins University, Baltimore), was used in some experiments. DBNBS in solution exists in a monomer−dimer equilibrium, and only the monomeric form of DBNBS is suitable for spin trapping. The equilibrium constant (K_d = [monomer]^2/[dimer]) at 25 °C is 1.3×10^{-3} mol/L, and the molar extinction coefficient of DBNBS monomer in water at 760 nm is equal to 34 L mol^{-1} cm^{-1}).[22] In pure DMF, DBNBS is present predominantly in its monomeric form at low concentrations. The maximum absorbance of DBNBS-monomer is shifted to 780 nm and follows the Lambert−Beer law up to 5 mg/mL (total dissolved DBNBS). A deviation from this linearity was only observed at higher concentrations (>10 mg/mL) of DBNBS. The extinction coefficient of DBNBS-monomer in DMF, calculated from the data at low DBNBS concentration, was found to be equal to 34.3 L mol^{-1} cm^{-1} and was identical within an experimental error with the extinction coefficient of DBNBS-monomer in water at 760 nm.[22] Thus, an extinction coefficient of 34 L mol^{-1} cm^{-1} at the maximum of the absorbance in the 760−780-nm region was used to calculate the amount of DBNBS-monomer in the DMF/water mixtures.

Sonolysis Experiment. The aqueous mixtures (1.7 mL) of DMF containing 3 mg/mL DBNBS (total monomer+dimer) were sonicated in Pyrex 13 × 100 mm disposable tubes (Corning Inc., New York) fixed in the center of a sonication bath (Bransonic 1200) with a frequency of 50 kHz. The temperature of the coupling water was 25 °C. The sample was sealed with a rubber septum and bubbled with argon through a Teflon tube attached to a fine needle (the argon flow rate was 50 mL/min) for 5 min before and during sonication. In a typical experiment, the sample was removed for EPR measurement after 10 min of sonolysis.

For comparison, sonolysis of 1.7 mL of aqueous argon-bubbled ferrous sulfate Fricke dosimeter solution[23] under the same conditions gave an absorbance reading of 0.536 ± 0.050 (seven determinations) at 302 nm in a 1-cm cell.

We found that the reproducibility of the sonochemical experiments improved significantly (results of repeated experiments are usually within ±10%) when a new test tube was used for every experiment. With repeated use of the same tube the sonochemical yields (measured by Fricke dosimetry) gradually decreased until they leveled off after about four runs at a value approximately one-third of the first experiment. We presume that this difference was due to the initial presence of crevices filled with gas in the walls of the test tubes that could serve as cavitation nuclei. With repeated experiments in the same tube, the gas was expelled from the crevices in the tube walls, resulting in decreased cavitation.

EPR Measurements. Immediately after sonication, degassed organic liquids were transferred under a nitrogen atmosphere to EPR quartz flat cells to eliminate line-width broadening due to the presence of dissolved oxygen. A Varian E-9 X-band spectrometer with 100-kHz modulation frequency and a microwave power of 20 mW was used to record the spectra for both sonolysis and photolysis experiments. The EPR software EPRDAP, written by Dr. P. Kuppusamy (U. S. EPR, Inc., Clarksville, MD), was used for acquisition, analysis, and simulation of EPR data.

Photolysis Experiments. Hydroxyl radicals formed by photolysis of H_2O_2 (305 ± 10 nm light) were used to produce hydrogen atom abstraction radicals from organic solvents. Ten microliters of 30% H_2O_2 were added to 300 μL of aqueous mixtures of DMF in the presence of 3 mg/mL DBNBS. Samples were illuminated *in-situ* in the cavity of the EPR spectrometer for 2−5 min and the EPR spectra were recorded. Control experiments were performed in each case, to determine any radicals formed by direct photolysis of the solvent.

The photolysis experiments were carried out at room temperature using a Schoeffel 1000-W xenon lamp coupled to a Schoeffel grating monochromator.

Results and Discussion

Identification of the Spin-Trapped Radicals. A typical spectrum of radical adducts obtained by sonication of argon-saturated aqueous solutions of DMF in the presence of the spin trap DBNBS is shown in Figure 2a. This spectrum is a mixture of two signals: the dominant component is the spectrum of the methyl radical adduct of DBNBS (DBNBS/$^{\bullet}CH_3$; simulation of this signal is shown in Figure 2b); the second component (the overlapping multiline signal) was obtained in almost pure form by H_2O_2 photolysis in aqueous DMF mixtures (Figure 2c). This spectrum was therefore tentatively assigned to the signal of the $^{\bullet}CH_2N(CH_3)CHO$ adduct of DBNBS, which is produced by $^{\bullet}OH$ radical abstraction from DMF. A satisfactory isotropic simulation of DBNBS/$^{\bullet}CH_2N(CH_3)CHO$ (Figure 2c) could not be obtained using the splitting constants obtained for the

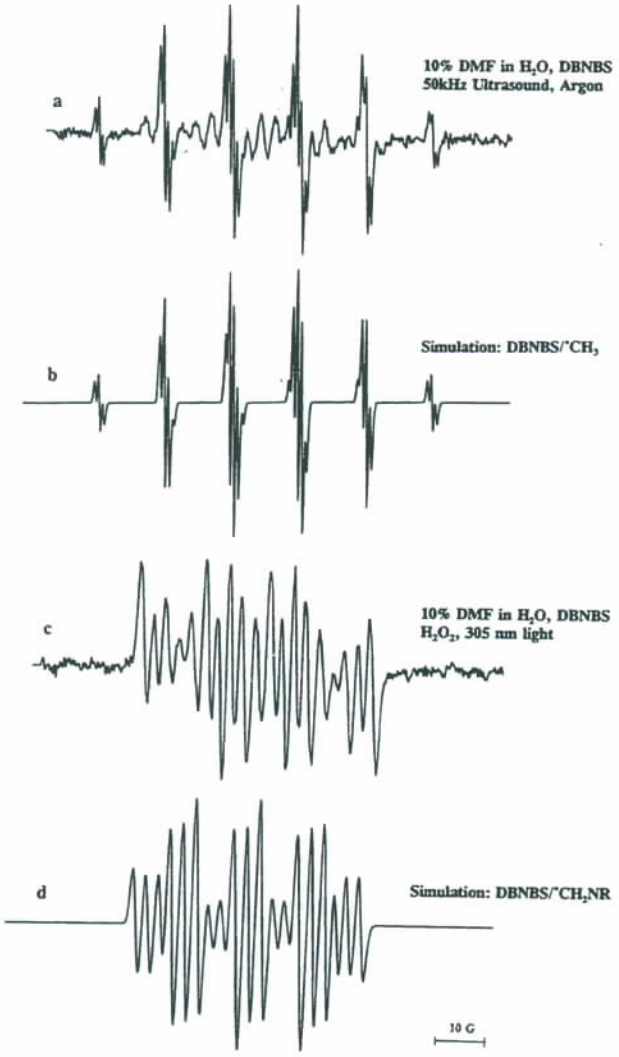

Figure 2. (a) EPR spectrum obtained by 50-kHz sonolysis (10 min) of 10% aqueous *N,N*-dimethylformamide (DMF) under argon gas in the presence of 8.2 mmol/L DBNBS. Instrumental conditions: modulation amplitude 0.063 mT, time constant 0.250 s, scan time 240 s, microwave power 20 mW, gain 8×10^4. (b) Simulation of the spectrum of DBNBS/•CH_3. Splitting constants used in simulation: $a_N = 1.423$ mT, $3a_H = 1.3306$ mT, $2a_H^m = 0.075$ mT; line width 0.06 mT. (c) EPR spectrum obtained by 305-nm photolysis (120-s irradiation time) of 1% H_2O_2 in 10% DMF in water in the presence of 8.2 mmol/L DBNBS. Instrumental conditions are the same as in Figure 2a. (d) An attempt to simulate spectrum c (DBNBS/•$CH_2N(CH_3)CHO$ adduct) using correspondingly adjusted splitting constants obtained from photolysis experiments with DMF-d_7 (see Figure 3): $a_N^1 = 1.3326$ mT, $a_N^2 = 0.255$ mT, $2a_H = 0.741$ mT; line width 0.16 mT.

DBNBS/•$CD_2N(CD_3)CDO$ adduct (see the following paragraph) with the correspondingly adjusted two methylene hydrogen splittings (Figure 2d); although this simulation has the same number of lines as the experimental spectrum (Figure 2c) and almost identical position of the peaks, it fails to reproduce the relative line widths and peak intensities of the original spectrum. This phenomenon is caused by hindered rotation of the methylene group and will be discussed later.

To confirm the identification of the radical formed by hydrogen abstraction from DMF, photolysis experiments were performed with deuterated DMF (DMF-d_7). The EPR spectrum of the DBNBS adduct formed by spin trapping of radicals formed by deuterium abstraction by •OH radicals from DMF-d_7 is shown in Figure 3a. The signal consists of a mostly unresolved triplet. The following experiments demonstrate that this signal can be assigned to a DBNBS/•CD_2N-type adduct.

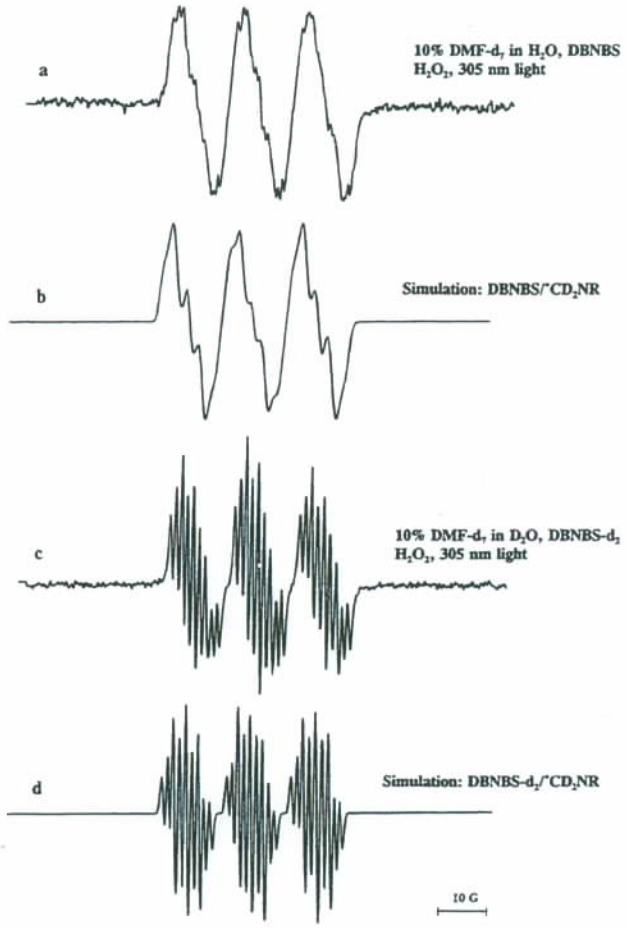

Figure 3. (a) EPR spectrum obtained by 305-nm photolysis (120-s irradiation time) of 1% H_2O_2 in the presence of 10% DMF-d_7 in H_2O in the presence of 8.2 mmol/L DBNBS. Instrumental conditions are the same as in Figure 2a. (b) Simulation of the DBNBS/•CD_2R adduct signal (trace a). Splitting constants used in simulation: $a_N^1 = 1.3326$ mT, $a_N^2 = 0.255$ mT, $2a_D = 0.1138$ mT; line width 0.16 mT (unresolved splittings from the *meta*-hydrogens of DBNBS contribute to the line width). (c) EPR spectrum obtained by 305-nm photolysis (120-s irradiation time) of 1% H_2O_2 in 10% DMF-d_7 in D_2O in the presence of 8.2 mmol/L DBNBS-d_2. Instrumental conditions are listed in Figure 2a; gain 1×10^5. (d) Simulation of the DBNBS-d_2/•CD_2R adduct (trace c). Splitting constants used in simulation: $a_N^1 = 1.3326$ mT, $a_N^2 = 0.255$ mT, $2a_D = 0.1138$ mT; line width 0.05 mT.

The signal resolution increased markedly when the deuterated form of the spin trap (DBNBS-d_2) is used in the same experiment performed in D_2O (Figure 3c). (The enhanced resolution is due to the fact that the small DBNBS-*meta*-hydrogen splittings, which did not fully resolve but which contributed to the line width, decreased by a factor 6.51 (the gyromagnetic ratio H/D) by replacing them with deuterium.) This spectrum could be simulated (Figure 3d) using one nitrogen splitting constant of 1.33 mT, another smaller nitrogen splitting constant (0.255 mT) and two equivalent deuterium splittings (0.11 mT). On the basis of this result, the spectrum obtained in the photolysis experiment (Figure 3c) was assigned to the •$CD_2N(CD_3)CDO$ adduct of DBNBS-d_2, which was formed by deuterium abstraction from DMF-d_7 by •OH radicals. When the simulation parameters from Figure 3d were used along with a larger line width (due to the unresolved splittings from the *meta*-hydrogens of the spin trap), a satisfactory fit of the experimental spectrum in Figure 3a was obtained (Figure 3b).

As already mentioned earlier, the attempted simulation of the DBNBS/•$CH_2N(CH_3)CHO$ signal using correspondingly adjusted splittings of the •$CD_2N(CD_3)CDO$ adduct of DBNBS was

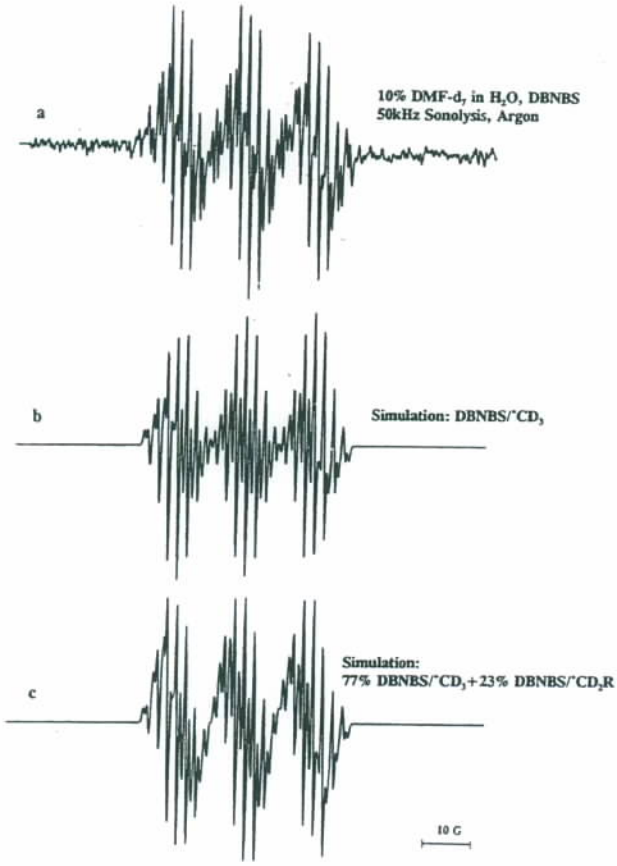

Figure 4. (a) EPR spectrum obtained by 50-kHz sonolysis (10 min) of 10% aqueous *N,N*-dimethylformamide-d_7 (DMF-d_7) under argon gas in the presence of 8.2 mmol/L DBNBS. Instrumental conditions: modulation amplitude 0.063 mT, time constant 0.128 s, scan time 120 s, microwave power 20 mW, gain 6.3×10^4. (b) Simulation of the spectrum of the DBNBS/$^{\bullet}CD_3$ adduct. Simulation parameters: $a_N = 1.4234$ mT, $3a_D = 0.2044$ mT, $2a_H^m = 0.075$ mT; line width 0.06 mT). (c) Simulation of the complete spectrum a. The resulting spectrum is a composite of two spectra: 77% DBNBS/$^{\bullet}CD_3$ (Figure 4b) and 23% DBNBS/$^{\bullet}CD_2R$ (Figure 3b).

not successful. This is due to the distortion of the spectrum caused by the hindered rotation of the methylene group of the $^{\bullet}CH_2N(CH_3)CHO$ radical attached to the nitrogen group of the spin trap, which results in nonequivalence of the methylene-hydrogen splittings and line-width alternations. This effect was originally described by Lagercrantz and Setaka[24] for the nitroso-*tert*-butyl/$^{\bullet}CH_2R$-type adducts produced by hydrogen abstraction from *N,N*-dimethylformamide, *tert*-butyl alcohol, 2,2-dimethylpropanoic acid, 5,5-dimethylhydantoin, 5-methylhydantoin, isopropyl alcohol, and 3-hydroxy-2-methylpropanoic acid. Contrary to the results obtained for DMF, in experiments using deuterated DMF-d_7 the observed spectrum of the $^{\bullet}CD_2N(CD_3)$-CHO adduct (Figure 3c) can be reproduced using isotropic simulation with two equivalent methylene-deuterium splittings (Figure 3d). This suggests a difference in the rotational barrier between the CH_2 and CD_2 groups of the spin adducts. Similar differences in the rotational barrier of the CH_2 and CD_2 groups in 3-*tert*-butyl nitrosobenzene/$^{\bullet}CH_2N(CH_3)CHO$ and $^{\bullet}CD_2N$-$(CH_3)CHO$ radical adducts produced by hydrogen abstraction in pure DMF and DMF-d_7 were found previously.[25] A deuterium isotope effect on the rotational barrier was also reported by Fessenden[26] for $CHD_2CD_2^{\bullet}$ and $CH_3CH_2^{\bullet}$ and by Jensen and Smith[27] for cyclohexatriene.

An example of EPR spectra obtained by the sonolysis of 10% DMF-d_7 in the presence of DBNBS is shown in Figure 4a. As confirmed by spectral simulations (Figure 4b,c), this signal consists of two components: the dominant well-resolved signal is a spectrum of the DBNBS/$^{\bullet}CD_3$ adduct (simulation of this spectrum is shown in Figure 4b). (The splitting constants used for spectral simulation of the DBNBS/$^{\bullet}CD_3$ adduct were identical with those used for the simulation of DBNBS/$^{\bullet}CH_3$ except that the hydrogen splittings from the three methyl hydrogens were replaced by three deuterium splittings, each being 6.51 times (the gyromagnetic ratio of H/D) smaller than the corresponding hydrogen splitting.) The irregular shape of the spectrum in Figure 4a is caused by the presence of the broad triplet signal of DBNBS/$^{\bullet}CD_2N(CD_3)CDO$ (Figure 3a); the successful simulation was a composite of 77% DBNBS/$^{\bullet}CD_3$ and 23% DBNBS/$^{\bullet}CD_2N(CD_3)CDO$ (Figure 4c). Thus, our data show that $^{\bullet}CD_3$ and $^{\bullet}CD_2N(CD_3)CDO$ radical adducts of DBNBS are produced in the sonolysis of DMF-d_7. The experiments in deuterated DMF, therefore, confirm our assignment of the radicals spin trapped in sonolysis of DMF as $^{\bullet}CH_3$ and $^{\bullet}CH_2N(CH_3)CHO$.

In our previous studies on the sonolysis in 100% DMF, the $^{\bullet}CH_3$ and $^{\bullet}CH_2N(CH_3)CHO$ radicals were spin trapped using 2,4,6-tri-*tert*-butylnitrosobenzene[25] or nitrosodurene.[28] In addition to these dominant species, a weak signal of the $^{\bullet}C(O)N$-$(CH_3)_2$ adduct, produced by hydrogen abstraction from DMF, was detected using 2,4,6-tri-*tert*-butylnitrosobenzene,[25] and small amounts of $^{\bullet}N(CH_3)R$ radicals, produced by pyrolysis of one of the three weak C−N bonds in DMF, could be detected with nitrosodurene.[28] Relative yields of spin-trapped radicals in sonochemical studies are a function of the rate constants with the spin trap and the availability of the spin trap in different sonochemical regions (i.e. the less polar spin traps are likely to accumulate in the low-polarity interface, being thus able to trap radicals formed by pyrolysis in the hot cavitation region more efficiently, by outcompeting other processes for their removal). Our identification of the $^{\bullet}CH_2N(CH_3)CHO$ radical as the major hydrogen abstraction intermediate agrees with the results of Dusaucy et al. in γ-irradiated DMF;[29] using a dimer analysis in γ-irradiated solid DMF (77 K), they estimated that the radical distribution was 82−89% $^{\bullet}CH_2N(CH_3)CHO$ and 11−18% $^{\bullet}C$-$(O)N(CH_3)_2$ radical. They found that the relative yields of the $^{\bullet}CH_2N(CH_3)CHO$ radicals were even higher in γ-irradiated aqueous solutions of DMF. These results are in accord with the results of Hayon et al.,[30] who showed the high selectivity of the reaction

$$CH_3N(CH_3)CHO + {}^{\bullet}OH \rightarrow {}^{\bullet}CH_2N(CH_3)CHO \quad (1)$$

They suggested that this is due to the activation of the methyl groups by amide nitrogen (the rate constant of this reaction was found to be $(2.3 \pm 0.2) \times 10^9$ L mol^{-1} s^{-1} [30]). In general, the rate of $^{\bullet}OH$ abstraction from the *N*-methyl group of amides is at least 1 order of magnitude faster than from the methyl group attached to carbonyl carbon; this point is demonstrated clearly by comparison of the rate constants with $^{\bullet}OH$ radicals of acetamide and *N,N*-dimethylacetamide with acetic acid and its methyl ester: CH_3CONH_2, 1.9×10^8 L mol^{-1} s^{-1}; CH_3CON-$(CH_3)_2$, 3.5×10^9 L mol^{-1} s^{-1}; CH_3CO_2H, 1.4×10^7 L mol^{-1} s^{-1}; $CH_3CO_2CH_3$, 8×10^7 L mol^{-1} s^{-1} [30].

Spin Trapping Efficiency. In order to estimate the efficiency of spin trapping of the radicals produced in DMF, the DBNBS concentration dependence on the yields of spin-trapped radicals was studied (Figure 5). The observed concentration dependence is a result of a complex competition of the spin trap with the

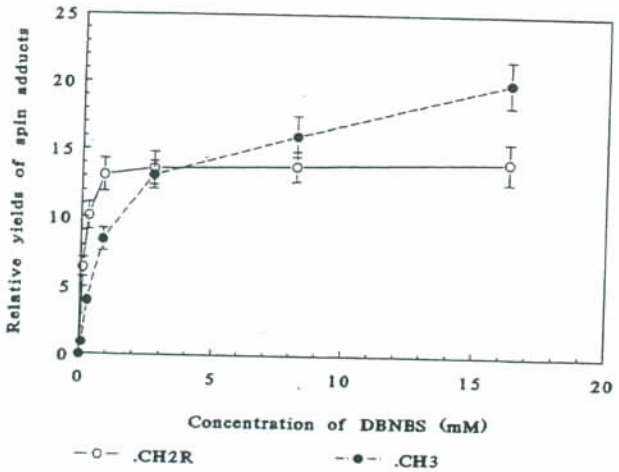

Figure 5. DBNBS concentration dependence of the DBNBS/$^{\bullet}CH_2R$ and DBNBS/$^{\bullet}CH_3$ adduct formation in 100% DMF. The relative concentrations of the $^{\bullet}CH_2R$ and $^{\bullet}CH_3$ adducts (expressed in arbitrary units) are approximate and were determined from the relative peak–peak EPR signal intensities of the two signals corrected for the line width and the line multiplicity. The EPR data were obtained using the experimental conditions listed in Figure 2a.

radical reactions in the system:

$$CH_3N(CH_3)CHO \xrightarrow{)))} {}^{\bullet}CH_3 + {}^{\bullet}N(CH_3)CHO \quad (2)$$

$$CH_3N(CH_3)CHO + {}^{\bullet}CH_3 \rightarrow {}^{\bullet}CH_2N(CH_3)CHO + CH_4 \quad (3)$$

$${}^{\bullet}CH_3 + {}^{\bullet}CH_3 \rightarrow CH_3CH_3 \quad (4)$$

$${}^{\bullet}CH_2N(CH_3)CHO + {}^{\bullet}CH_3 \rightarrow \text{nonradical products} \quad (5)$$

$${}^{\bullet}CH_2N(CH_3)CHO + {}^{\bullet}CH_2N(CH_3)CHO \rightarrow \text{nonradical products} \quad (6)$$

$$DBNBS + {}^{\bullet}CH_3 \rightarrow DBNBS/{}^{\bullet}CH_3 \quad (7)$$

$$DBNBS + {}^{\bullet}CH_2N(CH_3)CHO \rightarrow DBNBS/{}^{\bullet}CH_2N(CH_3)CHO \quad (8)$$

As seen from Figure 5, the spin trap reaches almost 100% efficiency in trapping of $^{\bullet}CH_2N(CH_3)CHO$ radicals already at 1–2 mmol/L concentration (for comparison, the DMF concentration in 100% DMF is 12.9 mol/L). In contrast, the trapping efficiency of $^{\bullet}CH_3$ radicals did not reach 100% even at the highest concentration of DBNBS used (16.5 mmol/L). The reason may be partially due to the higher reactivity of methyl radical compared to $^{\bullet}CH_2N(CH_3)CHO$ radicals and also to the sonochemical compartmentalization of the sonochemical reactions: whereas the amphiphatic nature of DMF allows its effective accumulation at the bubble interface (see discussion in the Introduction), the charged DBNBS molecule is not likely to be present in this region at the same concentration as in the bulk solution and thus may be unable to compete with other modes of $^{\bullet}CH_3$ radical removal (eqs 3–5), particularly the recombination (eq 4).

The results shown in Figure 5 also demonstrate that sonolysis of the spin trap does not contribute to the yield of the abstraction radicals ($^{\bullet}CH_2N(CH_3)CHO$). The possibility that the weak C–NO bond of the spin trap (215.5 and 211.3 kJ/mol for similar aromatic nitroso compounds, nitrosobenzene and pentafluoronitrosobenzene, respectively)[31] may be subject to thermolysis was investigated recently.[28] The resulting phenyl radicals might abstract hydrogen from DMF, thus forming the $^{\bullet}CH_2N(CH_3)CHO$ radicals. If this were the case, however, the levels of spin trapped $^{\bullet}CH_2N(CH_3)CHO$ radical would not level off but would continue to grow with increasing concentration of the spin trap.[28]

DMF Concentration Dependence of Radical Production by Sonolysis. Using 8.2 mmol/L DBNBS the signals of $^{\bullet}CH_3$ and $^{\bullet}CH_2N(CH_3)CHO$ adducts could be detected throughout the whole concentration range of DMF (0.004–12.9 mol/L; or DMF mole fraction 7×10^{-5} to 1) (Figure 6). The methyl radicals are typical pyrolysis products of DMF produced by the thermal cleavage of the weak C–N bond (eq 2). The other spin-trapped radical, $^{\bullet}CH_2N(CH_3)CHO$, is produced at low DMF concentrations by hydrogen atom abstraction from DMF by $^{\bullet}OH$ radicals or $^{\bullet}H$ atoms generated by sonolysis of H_2O:

$$H_2O \xrightarrow{)))} {}^{\bullet}OH + {}^{\bullet}H \quad (9)$$

$$CH_3N(CH_3)CHO + {}^{\bullet}OH \rightarrow {}^{\bullet}CH_2N(CH_3)CHO + H_2O \quad (1)$$

$$CH_3N(CH_3)CHO + {}^{\bullet}H \rightarrow {}^{\bullet}CH_2N(CH_3)CHO + H_2 \quad (10)$$

Reaction 10 is not likely to contribute to the production of the abstraction radicals in our system because this reaction is too slow (its rate constant is on the order of 10^5 L mol^{-1} s^{-1}: a value of 1.9×10^5 L mol^{-1} s^{-1} is listed for acetamide)[32] to compete with the diffusion-limited ($\sim 10^{10}$ L mol^{-1} s^{-1}) radical recombination reactions with $^{\bullet}H$ atoms and $^{\bullet}OH$ radicals, present at high concentrations at the interfacial region. On the other hand, due the high rate constant of DMF with $^{\bullet}OH$ radicals ($k_{DMF/OH} = (2.3 \pm 0.2) \times 10^9$ L mol^{-1} s^{-1} [30]), DMF accumulated at the interfacial region is likely to outcompete the concurrent processes of $^{\bullet}OH$ removal. While the reaction with $^{\bullet}OH$ radicals may be the dominant pathway for the production of $^{\bullet}CH_2N(CH_3)CHO$ radicals at low DMF concentration, at high mole fraction of DMF, hydrogen abstraction by the methyl radical predominates, leading to the same radical (eq 3).

The DMF concentration dependence of the methyl and $^{\bullet}CH_2N(CH_3)CHO$ DBNBS adduct formation by ultrasound is different from those observed in our previous studies on the sonochemistry aqueous mixtures of volatile[19,20] and nonvolatile solutes.[33,34] For volatile solutes (acetone, acetonitrile, alcohols) after an initial rapid increase of the pyrolysis radicals with increasing solute concentration, the radical yields fall to zero at higher solute concentrations, which results from the decrease of the effective temperature of the collapsing cavitation bubbles due to the decrease of the effective γ (C_p/C_v) in the gas bubbles containing the vapors of the volatile solute. In the sonolysis of aqueous mixtures of nonvolatile solutes (i.e. sodium acetate, sodium propionate, amino acids, sugars) only the radicals formed by $^{\bullet}OH$ radical abstraction could be spin trapped with DBNBS at low solute concentrations, whereas the pyrolysis radicals (typically methyl) became detectable only at high solute concentrations (>0.1 mol/L and in most cases >0.5 mol/L). DMF represents the special case of a solute which is freely miscible with water and at the same time is a good solvent for low-polarity solvents such as aromatic hydrocarbons, and its vapor pressure is lower than that of water (see below). These features allow DMF to accumulate in the interfacial region of the cavitation bubbles, resulting in detectable yields of the pyrolysis product $^{\bullet}CH_3$ at low DMF concentrations (4 mmol/L; Figure 6), with no dampening of the cavitation at high DMF concentrations (Figure 6, right panel), which was a prominent

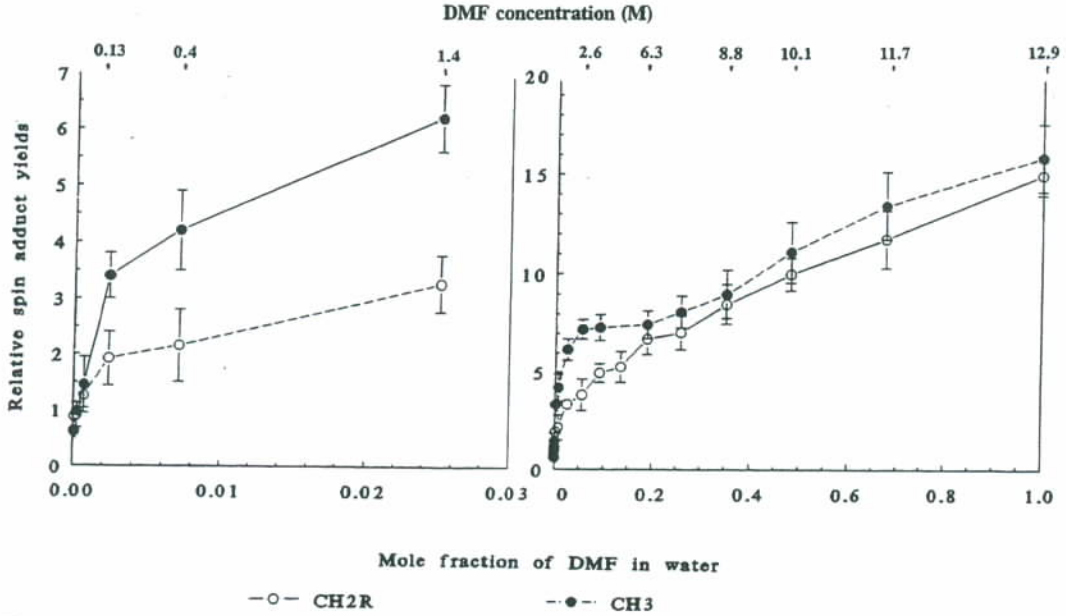

Figure 6. DMF concentration dependent formation of DBNBS/$^{\bullet}CH_2R$ and DBNBS/$^{\bullet}CH_3$ adducts in aqueous DMF solutions exposed to 50-kHz ultrasound under argon. The left panel shows the enlarged low-DMF-concentration region. The relative concentrations of the $^{\bullet}CH_2R$ and $^{\bullet}CH_3$ adducts (expressed in arbitrary units) are approximate and were determined from the relative peak−peak EPR signal intensities of the two signals corrected for the line width and the line multiplicity. The EPR data were obtained using the experimental conditions listed in Figure 2a.

feature in the solutes with high vapor pressures.[19,20] Thus, increased availability of DMF molecules both for pyrolysis and for hydrogen abstraction reactions at higher mole fractions of DMF and the lower vapor pressure of DMF (3.7 Torr at 25 °C) compared to water (24 Torr at 25 °C) are most likely the factors responsible for the continuing increase of the sonochemical radical yields at high DMF concentrations. Among other factors that favor maximum acoustic cavitation are (i) low viscosity (0.802 cP for DMF, 0.9 cP for water; 25 °C), (ii) high surface tension (35.2 dyn/cm for DMF; 72 dyn/cm for H_2O; 25 °C), (iii) high sound velocity (1460 m s^{-1} for DMF; 1497 m s^{-1} for water, at 25 °C), (iv) high γ (C_p/C_v)(~1.2 for DMF; ~1.3 for H_2O at 25 °C)[35] (with the exemption of monoatomic gases, the specific heats C_p and C_v and their ratio γ are a function of temperature: γ of the water vapor is equal to 1.31 at 25 °C and decreases to 1.17 at 1700 °C[35]) and (v) low thermal conductivity (1.84 kJ s^{-1} cm^{-1} K^{-1} for DMF; 2.30 kJ s^{-1} cm^{-1} K^{-1} for H_2O; 23.5 °C).

Apart from the parameters that affect the cavitation yields at different DMF concentrations, the observed continuing increase of the radical yields with the increasing mole fraction of DMF (Figure 6) could be due to the increasing availability of the monomeric form of the spin trap (which is the form suitable for spin trapping) with increasing concentration of DMF (Figure 7). We can exclude this possibility on the basis of the results in Figure 5, which show an almost 100% efficiency of trapping of $^{\bullet}CH_2N(CH_3)CHO$ radicals with 1 mmol/L (and higher) monomer of DBNBS in pure DMF. At the high concentrations of DMF, the dominant reaction for $^{\bullet}CH_2N(CH_3)CHO$ radical formation is

$$Ch_3N(CH_3)CHO + {}^{\bullet}CH_3 \rightarrow {}^{\bullet}CH_2N(CH_3)CHO + CH_4 \quad (3)$$

Hence, it follows that the increasing yields of DBNBS/$^{\bullet}CH_2N(CH_3)CHO$ with increasing mole fraction of DMF cannot be due to the increased availability of the DBNBS-monomer but must be due to the enhanced production of methyl radicals. Thus, we conclude that with increasing mole fraction of DMF in water the sonochemical radical yields are increasing, due in part to the increased availability of DMF molecules for pyrolysis and radical abstraction reactions and also due to the lower vapor pressure of DMF compared to water.

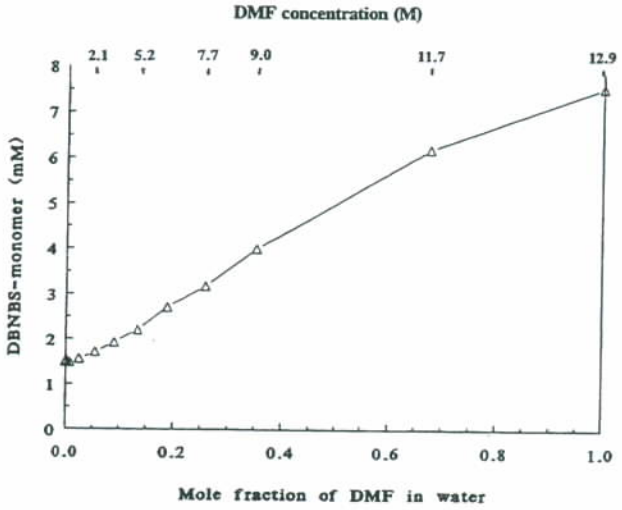

Figure 7. Dependence of the DBNBS-monomer concentration on the mole fraction of DMF in water. Total DBNBS concentration in all samples was 8.2 mmol/L. The concentration of DBNBS-monomer was determined from the measurement of optical densities in the 760−780-nm region (details in the Experimental Section).

Acknowledgment. We wish to thank Dr. Heasook Kim for assisting with preliminary measurements.

References and Notes

(1) Boudjouk, P. *J. Chem. Educ.* **1986**, *63*, 427.
(2) Ando, T.; Kimura, T. *Adv. Sonochem.* **1991**, *2*, 211.
(3) Price, G. J., (Ed.) *Current Trends in Sonochemistry*; Royal Society of Chemistry: Cambridge, U.K., 1992.
(4) Mason, T. J.; Lorimer, J. P. *Sonochemistry: Theory, Applications and Uses of Ultrasound in Chemistry*; Ellis Horwood: Chichester, U.K., 1988.
(5) Kittila, R. S. *Dimethylformamide Chemical Uses*; E. I. Du Pont de Nemours & Co.: Wilmington, DE, 1967.
(6) Jeffers, R. J.; Freng, R. Q.; Morse, P. D., II; Fowlkes, J. B.; Kessel, D.; Cain, C. A. *J. Acoust. Soc. Am.* **1995**, *97*, 669.

(7) Cain, C. A.; Jeffers, R. J.; Feng. R. Q.; Fowlkes, J. B.; Kessel, D. *Ultrasound Med. Biol.* **1994**, *20* (Suppl. 1), S96.
(8) Suslick, K. S.; Hammerton, D. A.; Cline, R. E., Jr. *J. Am. Chem. Soc.* **1986**, *108*, 5641.
(9) Flint, E. B.; Suslick, K. S. *Science* **1991**, *253*, 1397.
(10) Suslick, K. S.; Kemper, K. A. Pressure Measurements During Acoustic Cavitation by Sonoluminescence. In *Bubble Dynamics and Interface Phenomena*; Blake, J. R., Thomas, N., Eds.; Kluwer Publishers: Dordrecht, Netherlands, 1994; pp 311−320.
(11) Riesz, P.; Kondo, T. *Free Radical Biol. Med.* **1992**, *13*, 247.
(12) Franck, E. U. *J. Chem. Thermodyn.* **1987**, *19*, 225.
(13) Henglein, A.; Kormann, C. *Int. J. Radiat. Biol.* **1985**, *48*, 254.
(14) Alegria, A. E.; Lion, Y.; Kondo, T.; Riesz, P. *J. Phys. Chem.* **1989**, *93*, 4908.
(15) Henglein, A. *Ultrasonics* **1987**, *25*, 6.
(16) Suslick, K. S. *Science* **1990**, *247*, 1439.
(17) Riesz, P.; Berdahl, D.; Christman, C. L. *Environ. Health. Perspect.* **1985**, *64*, 233.
(18) Suslick, K. S.; Gawienowski, J. J.; Schubert, P. E.; Wang, H. H. *Ultrasonics* **1984**, *22*, 33.
(19) Riesz, P.; Kondo, T.; Carmichael, A. J. *Free Radical Res. Communs.* **1993**, *19*, S45.
(20) Krishna, C. M.; Kondo, T.; Riesz, P. *J. Phys. Chem.* **1989**, *93*, 5166.
(21) Kondo, T.; Kirschenbaum, L. J.; Kim, H.; Riesz, P. *J. Phys. Chem.* **1993**, *97*, 522.
(22) Ide, H.; Hagi, A.; Ohsumi, S.; Murakami, A.; Makino, K. *Biochem. Int.* **1992**, *27*, 367.
(23) Spinks, J. W. T.; Woods, R. J. *An Introduction to Radiation Chemistry*, 2nd ed.; John Wiley & Sons: New York, 1976.
(24) Lagercrantz, C.; Setaka, M. *Acta Chem. Scand.* **1974**, *B28*, 619.
(25) Mišík, V.; Riesz, P. *J. Phys. Chem.* **1994**, *98*, 1634.
(26) Fessenden, R. W. *J. Chim. Phys. Phys.−Chim. Biol.* **1964**, *61*, 1570.
(27) Jensen, F. R.; Smith, L. A. *J. Am. Chem. Soc.* **1964**, *86*, 956.
(28) Mišík, V.; Riesz, P. *Ultrason.-Sonochem.* **1994**, in press.
(29) Dusaucy, A.-C.; De Doncker, J.; Couillard, C.; De Laet, M.; Tilquin, B. *J. Chem. Soc., Faraday. Trans. 1* **1987**, *83*, 125.
(30) Hayon, E.; Ibata, T.; Lichtin, N. N.; Simic, M. *J. Am. Chem. Soc.* **1970**, *92*, 3898.
(31) Choo, K. Y.; Golden, D. M.; Benson, S. W. *Int. J. Chem. Kinet.* **1975**, *7*, 713.
(32) Neta, P.; Fessenden, R. W.; Schuler, R. H. *J. Phys. Chem.* **1971**, *75*, 1654.
(33) Kondo, T.; Krishna, C. M.; Riesz, P. *Radiat. Res.* **1989**, *118*, 211.
(34) Kondo, T.; Krishna, C. M.; Riesz, P. *Int. J. Radiat. Biol.* **1990**, *57*, 23.
(35) Zemansky, M. W. *Heat and Thermodynamics*; McGraw-Hill Book Co., Inc.: New York and London, 1943; p 104.

JP942433S